Loss of galactan synthesis in pea (Pisum sativum) causes defects in organ expansion and is associated with increased extensin content

Xiaoyuan Guo
University of Copenhagen
Ajay Kumar
Slovak Academy of Sciences
Ida Elisabeth Johansen
University of Copenhagen
Jesper Harholt
University of Copenhagen
William Willats
Newcastle University
Peter Ulvskov
University of Copenhagen
Jozef Mravec
jozef.mravec@savba.sk

Slovak Academy of Sciences

Research Article

Keywords: Pisum sativum, cell elongation, β-1,4-galactan, extensin, virus-induced gene silencing, microarray polymer profiling, monoclonal antibody, gene expression

Posted Date: April 1st, 2026

DOI: https://doi.org/10.21203/rs.3.rs-9136352/v1

Additional Declarations: No competing interests reported.

Abstract

Pectic galactan is a rhamnogalacturonan-I side chain, composed of β-1,4-linked D-galactose residues. Its multifunctional role in cell wall assembly and properties has primarily been proposed in various developmental contexts. In this study, we investigated the role of galactan in pea (*Pisum sativum syn. Lathyrus oleraceus*). First, we used glycan profiling to examine stems with different auxin-induced elongation rates for changes in cell wall composition. The galactan epitopes, recognised with the LM5 monoclonal antibody, were more abundant in the convex, more elongated part of the pea stem. This finding was supported by monosaccharide composition analysis and epitope detection chromatography (EDC). To evaluate the impact of disrupting galactan synthesis on pea development, we used Virus-Induced Gene Silencing (VIGS) to downregulate the pea ortholog of Arabidopsis β-1,4-galactosyltransferases of the GT92 family (*PsGALS3*). Plants with silenced *PsGALS3* exhibited severe defects in elongation and vegetative organ growth. Microarray polymer profiling (MAPP) revealed that, alongside the reduction in galactan epitopes, the cell wall proteoglycan extensin content increased in these plants, as confirmed by *in situ* immunohistological analysis. Our results provide new evidence linking galactan to cell and organ expansion and the relation between pectin and structural cell wall glycoproteins, specifically extensin.

Key message

Mimicking auxin-driven tropic responses and virus-induced silencing of the pea orthologues of the galactan synthase gene indicate that cell wall galactan is required for organ elongation and expansion.

Introduction

The plant cell wall is a distinctive feature that encases and supports the cell, serving as the main barrier against pathogens and environmental stressors (Geitman, 2023; Cosgrove, 2024). Its diverse composition and complex 3D structure enable the wall to participate in various cellular functions (Zhang et al., 2025). Cell elongation is essential for plant development and growth. For cells to expand, the relatively rigid extraprotoplasmic structure must be adjusted; the degree and type of these adjustments vary depending on the cellular and developmental context (Labavitch, 1981; Cosgrove, 2024).

The plant hormone auxin, primarily in the form of indole-3-acetic acid (IAA), plays a crucial role in developmental and directional elongation during tropic responses (Du et al., 2020). It has long been understood that auxin activity is mediated through the modulation of apoplast pH and the dynamic interaction of glucan polymers, as described by the acid growth hypothesis (Hager et al., 1971; Labavitch & Ray, 1974; Kumar et al., 2025). Besides pH changes, cell wall components undergo compositional and structural dynamics; for example, the complexity of xyloglucan is regulated by auxin during different elongation programs (Velasquez et al., 2021; Aryal et al., 2020). The roles of other cell wall components in elongation have been suggested but remain poorly understood. This is especially true for pectic glycans and cell wall glycoproteins. Galactan chains, composed of (1,4)-linked β-D-*Gal*p units together

with α-1,5-arabinan and arabinogalactan, are three types of pectic rhamnogalacturonans I (RGI) side chains (Anderson & Pelloux, 2025). RGI is connected to homogalacturonan at least at the reducing end of the backbone but probably at both ends (Coenen et al., 2007). However, RGI is also involved in supramolecular complexes in which covalent linkages between RGI, AGP, and xylan have been demonstrated (Tan et al., 2013). Galactan sidechains play an important architectural role in secondary walls, where galactans appear to compete with xyloglucan for binding to cellulose microfibrils (Gao et al., 2023). RGI sidechains are modulated in primary walls. These components are upregulated during the transition from cell proliferation to cell elongation (Catalá et al., 1997; Willats et al., 1999), as observed in suspension-cultured carrot cells. Furthermore, previous *in situ* localisation studies have shown that galactan is restricted to the transition zone of the Arabidopsis root tip during rapid cell elongation (McCartney et al., 2003; Willson et al., 2015).

Rapid turnover of the pool of galactose in the wall is characteristic of the elongation zone, but the rate of turnover was not found to change upon auxin stimulation of cell expansion (Labavitch & Ray, 1974). The elongation zone is characterised by a higher level of cell wall hydration than in cells in which expansion has ceased (Goldberg et al., 1989); the length of galactan sidechains has also been implicated in both hydration and the mechanical properties of cell walls (Ulvskov et al., 2005). The lobing observed in many epidermal anticlinal cell walls appears to depend on local differences in mechanical properties, mediated by differential galactan deposition (Majda et al., 2017).

Galactan is synthesised in the Golgi apparatus by β-1,4-galactosyltransferases (GALS) of the GT92 family (Amos & Mohnen, 2019). These glycosyltransferases have been identified in Arabidopsis and are described both enzymatically and structurally (Liwanag et al., 2012; Ebert, 2018; Laursen et al., 2018; Prabhakar et al., 2023). Interestingly, Arabidopsis *gals* single and multiple mutants do not exhibit any striking developmental phenotypes (Liwanag et al., 2012; Ebert et al., 2018; Prabhakar et al., 2023). Galactan side-chain initiation and elongation are probably not both catalysed by GALS, as early biochemical work suggests the involvement of multiple activities (Goubet & Morvan, 1994; Geshi et al., 2002). GALS is involved in galactan elongation, but it is not known how many activities are involved in the assembly of the RGI galactan sidechains.

In our study, we used pea (*Pisum sativum* or recently introduced syn. *Lathyrus oleraceus*), a classic model for auxin-mediated control of cell elongation (Matchett and Nance, 1962; Labavitch and Ray, 1974; Gilkes & Hall, 1977; Bret-Harte and Talbott, 1993; Sauer et al., 2006). One advantage of pea is that it is highly amenable to auxin manipulation and provides ample material for analysis of cell wall composition. Additionally, a well-established protocol for virus-induced gene silencing (VIGS) is available (Grønlund et al., 2010). This provided an opportunity to investigate the roles of different cell wall components in elongation. Our results confirm that galactan is upregulated in cells undergoing auxin-triggered elongation. Unlike in *Arabidopsis*, the loss of galactan synthesis in pea results in distinct phenotypes and is accompanied by changes in the abundance of other cell wall components, namely, extensins.

Results

Galactan epitopes are regulated in IAA-induced differential elongation of the stem

We previously reported an experimental setup that induces pea stem curvature, mimicking tropic responses, by the unilateral application of an auxin-containing lanolin paste. This setup enables compositional analysis of cell wall dynamics underlying auxin-mediated differential organ elongation (Velasquez et al., 2021). Unlike the traditional approach of incubating excised pea stem segments directly in auxin-supplemented solutions, this arrangement enables monitoring changes in a more native *in vivo* context. Applying lanolin paste containing IAA to one side of the decapitated pea stem induces differential elongation and curvature after three days (Fig. 1). Applying pure lanolin paste served as a control. The convex (more elongated) and concave (less elongated) parts are dissected with a razor blade and analysed using biochemical and immunological approaches.

We previously reported changes in xyloglucan epitopes (Velasquez et al., 2021). Using the same setup, we now analysed the gradual changes in the cell wall composition of opposing curvature regions at three time points—24, 48, and 72 hours—using monoclonal Microarray Polymer Profiling (MAPP; Bakshani et al., 2023), previously also known as Comprehensive Microarray Polymer Profiling (CoMPP; Moller et al., 2007). This involved (1) CDTA-chelate-assisted extraction to liberate more soluble cell wall components, and (2) NaOH extraction, which solubilises more recalcitrant cell wall, especially hemicellulosic components. Both extracts were printed onto nitrocellulose arrays, which were then probed with a panel of 14 anti-glycan monoclonal antibodies. The quantification showed that among the 14 epitopes, galactan epitopes (recognised by the LM5 mAb; Jones et al., 1997) were upregulated in the more elongated, convex part (Fig. 2A, B). The ratio of signals between convex and concave sites increased gradually, while extensin epitope levels (recognised by LM3 mAbs) remained relatively stable. The signal intensity of LM5 in the stems' pure lanolin paste was similar to that at the concave site (+/-3%), confirming changes triggered by IAA. The immuno-glycan profiles indicate that auxin application on the stem induces compositional changes in the affected cell walls, including galactan, which is upregulated in the elongation regions and reaches a maximum at 48h after IAA application.

Epitope detection chromatography and monosaccharide composition analysis correlate with MAPP profiling data

To determine whether the variations in LM5 epitope abundance detected with MAPP are due to quantitative differences or structural changes in galactan chains or their linkages to other cell wall components, we used epitope detection chromatography (EDC), which combines size-exclusion chromatography with ELISA (Cornuault et al., 2014). The EDC profiles of LM5 epitopes from convex and concave regions were similar, differing mainly in the relative abundance (Fig. 2C). This indicates that the differences are likely quantitative rather than modifications in the galactan structures that contain epitopes recognised by the LM5 mAb. Consistent with this, monosaccharide composition analysis of AIR using HPLC revealed increased levels of galactose in the convex part of the pea stem compared to the

control (Fig. 2D). Conversely, a notable reduction in glucose abundance was observed. The *in vitro* observations were confirmed by an *in situ* detection of the galactan epitope on longitudinal sections of auxin-stimulated stems (Fig. 2E, F). The LM5 epitope was found in the cell walls of auxin-engorged cells in the cortical tissue's convex site but was nearly absent in the concave part.

Identification of putative pea β-1, 4-galactosyltransferases

To identify targets for functional analysis, we searched public databases for orthologs of Arabidopsis β-1,4-galactan synthases (Liwanag et al., 2012; Ebert et al., 2018; Yan et al., 2021). Psat1g151680 and Psat0s2609g0040 exhibit approximately 61% amino acid sequence identity with At5G44670 (AtGALS2) and At4G20170 (AtGALS3). Compared to each other, both pea GALS have 71.6% sequence identity (Fig. 3). Psat1g151680 (hereafter designated as *PsGALS3*) is located on linkage group 1LG6 within the *Pisum sativum* Cameor v1a reference genome, specifically at positions 299,495,892 to 299,499,832 bp on the forward strand. This gene is 2,465 bp and encodes a 515-amino-acid-long protein. In comparison, Psat0s2609g0040 (hereafter designated as *PsGALS2*) is found on scaffold CAADHX020007802.1 (Cameor v1a primary assembly) at positions 45,424 to 49,542 bp on the forward strand. It spans 1,913 bp and encodes a protein of 500 amino acids.

In the phylogenetic analysis of GT92 GALS proteins, Arabidopsis and Pea clearly cluster into separate groups (Fig. 3A). In Arabidopsis, AtGALS2 and AtGALS3 form a strongly supported subclade, indicating these two proteins are very similar. In contrast, AtGALS1 branches off separately and is more divergent from AtGALS2 and AtGALS3, suggesting functional or evolutionary differences. The two Pisum paralogs form a distinct, legume-specific group. While Psat1g151680 and Psat0s2609g0040 have moderate bootstrap support compared to AtGALS, this suggests possible species-specific duplication or diversification within *P. sativum*. The clear separation between Arabidopsis and Pisum clusters matches the expected evolutionary distances between Brassicaceae and Fabaceae. Branch lengths reflect the estimated number of amino acid substitutions per site, with Psat0s2609g0040 showing slightly longer branches than Psat1g151680, indicating greater sequence divergence. Overall, the tree shows that GALS proteins have experienced lineage-specific expansions and diversification while keeping a conserved structure within GT92.

Multiple sequence alignment demonstrated strong conservation of key structural and catalytic motifs in GT92 galactan synthases. The domain architecture, depicted in Fig. 4, is based on Prabhakar et al. (2023) and UniProt annotations for AtGALS proteins. According to CATH classifications, GALS proteins include two primary domains: an N-terminal β-sandwich/Jelly-roll fold (CATH 2.60.40) and a C-terminal GT-A fold catalytic domain (CATH 3.90.550). Prabhakar et al. (2023) identified the N-terminal β-sandwich/Jelly-roll region as a CBM95 carbohydrate-binding module that interacts specifically with the RG-I backbone in Populus trichocarpa. Alignment results showed that the N-terminal transmembrane helix and the C-terminal GT-A fold catalytic domain are highly conserved across all Arabidopsis and Pisum sequences, consistent with their predicted Golgi localization as type II membrane proteins. Conversely, the CBM-like domain exhibited moderate conservation with species-specific variation,

suggesting functional divergence in carbohydrate recognition. Among Arabidopsis proteins, AtGALS2 and AtGALS3 were the most similar, while AtGALS1 was more divergent. The two pea paralogs also showed considerable similarity, with Psat0s2609g0040 being slightly more divergent. Overall, the alignment supports conserved catalytic activity with lineage-specific adaptations in substrate-interaction regions.

PsGALS3 is expressed in aerial organs

The presence of *PsGALS3* transcripts in the initial transcriptome assemblies indicated higher expression than the other putative genes and was therefore selected for further analysis. To analyse expression, we conducted qRT-PCR in eight different aerial plant parts and seedlings (Fig. 5). The highest expression was observed in tendrils, while the lowest was in older leaves. The results indicate expression throughout the aerial parts, with no distinct hot spot; expression occurs mainly in rapidly growing organs.

Silencing of the PsGALS3 gene in plants using VIGS results in severe growth defects

To elucidate the consequences of the loss of galactan synthesis on pea elongation, we used virus-induced gene silencing (VIGS) to downregulate the *PsGALS3*. The pea early browning virus (PEBV) binary vector system was used to complement VIGS, with a 463 bp cDNA fragment of *PsGALS3* inserted into pCAPE 2, which contains genes encoding the virus coat protein (Constantin et al., 2004, Fig. 6A, B). GFP gene insertion served as a control for the empty virus (*siGFP*). Using these constructs, we performed the silencing experiment as described previously (Grønlund et al., 2010). Three weeks after decapitation and infiltration, the second internodes were analysed for PsGALS3 expression using semi-quantitative reverse transcriptase PCR (Semi-qRT-PCR) and real-time PCR(RT-qPCR) to validate the silencing efficiency. The expression data showed that *PsGALS3* was successfully silenced to approximately 15% of its normal expression (Fig. 6C, D).

We analysed the phenotypes of si*PsGALS3* plants and compared them with those of non-treated wild-type and *siGFP* control plants. The si*PsGALS3* plants were severely stunted compared to the empty virus controls (Fig. 7), featuring up to 50% reductions of internode length (Fig. 7D). In addition to shortened internodes, *siPsGALS3* plants produced smaller leaves, shorter tendrils, and a reduced root system (Fig. 7B, C).

siPsGALS3 plants have significantly reduced galactan epitopes but largely remain sensitive to auxin paste

To assess silencing efficiency at the level of cell wall component abundance, we analysed cell wall composition of stems from silenced plants using MAPP and selected pectin- and glycoprotein-related mAbs. The results confirmed a strong reduction in LM5 galactan epitopes in *siPsGALS3* compared to controls, to approximately 30% (Fig. 7E). Extractable cellulose, homogalacturonan, and arabinan were not significantly changed. However, significant upregulation of LM3 and LM1 epitopes was noticeable. This experiment demonstrated the efficacy of the VIGS approach and the functional relationship

between the *PsGALS3* gene and galactan synthesis. Next, we tested the auxin response capacity of the *siPsGALS3* stems. As in the initial experiments, we applied auxin to pea stems, including wild-type and VIGS control plants. Although noticeably shorter, the first internodes of *siPsGALS3* plants bent overall similarly to WT and *siGFP* control plants after auxin stimulation, which suggests that bending occurs normally despite reduced galactan content, and they are still able to react to auxin. (Fig. 7F).

Visualising the effect of PsGALS3 silencing on galactan and extensin epitopes in situ

Comparing MAPP data on auxin-induced stem curvature and si*PsGALS3* pea plants revealed an opposing correlation between galactan and extensin epitopes. To confirm this correlation *in situ*, we performed immunolocalisation on the vibratome-generated transversal pea stem sections. In WT plants, probing with LM5 mAb showed labelling in pith parenchyma cells only. The LM3 signal was generally weak and confined to small patches. In silenced plants, LM5 labelling was almost completely diminished; on the other hand, LM3 labelling strongly increased, and the signal was mainly restricted to triangular cell junctions in the parenchyma tissue (Fig. 8).

Discussion

The dynamic changes in cell wall properties required to match developmental programmes involve modulating composition and the intricate spatiotemporal arrangement of various cell wall components. Cellular expansion and cell division are the primary processes that shape the plant body. It has long been proposed that a key factor determining cell wall extensibility is the reversible noncovalent interaction between hemicelluloses, specifically xyloglucan, and cellulose microfibrils (Cosgrove, 2024). This interaction is linked to auxin-triggered expansin activation via apoplast acidification (Fendrych et al., 2016). Other cell wall components are also crucial in making cell walls extensible while providing strength and supporting load-bearing functions. Pectin side chains and homogalacturonan (HG) modifications, especially demethylation, play a vital role in this process. Galactan epitopes are specifically localised to the Arabidopsis root tip's elongation zone by immunohistochemistry and glycan profiling (McCartney et al., 2003; Wilson et al., 2015) as well as in a monocot species such as rye (Petrova et al., 2022). Intriguingly, Arabidopsis mutants affected in galactan synthesis showed no dramatic phenotypes, except for an altered response to salt stress (Yan et al., 2021).

Our work aligns with the already reported notion that galactan has a functional role in organ expansion (Anderson and Pelloux, 2025). In our setup miming pea tropism, galactan was upregulated on the more elongated side of the auxin-induced curvature. Unlike in Arabidopsis, downregulating galactan has severe effects on pea growth, including inhibited stem elongation. It is important to bear in mind that not all type-I cell walls are the same. We have previously presented evidence that the cell wall of members of the fabid clade displays separability differences compared with members of the malvid clade to which Arabidopsis belongs (Fangel et al., 2024). In other words, if differences in polysaccharide separability are regarded as evidence for cell wall architectural differences, then Arabidopsis is not a valid model for pea

in all aspects. Galactan was one of the polymers that showed differences in partitioning (Fangel et al., 2024).

Extensins are *O*-glycosylated proteins that belong to the hydroxyproline-rich glycoproteins (HRGPs) superfamily. Extensin sidechains on hydroxyproline (Hyp) consist of one to four arabinose residues, while serine may carry a single galactose residue (Velasquez et al., 2011; Saito et al., 2014; Moussu, 2023a,b). Although our data suggest that extensins are upregulated upon loss of galactan, the functional relationship between these two cell wall components remains unclear, and we cannot exclude that the increased labeling observed in immunolocalization is, in part, due to better exposure of the extensin in the wall with truncated galactans (Markus et al., 2008). The non-ionic interaction between extensin and pectin has been identified (Nuñez et al., 2009), and its importance for cell wall integrity has been demonstrated (Velasquez et al., 2011). Numerous previous studies suggest that extensins may play a general role in the cell wall's response to stress. For example, extensin-coding genes are upregulated during mechanical stress in tension wood formation or in response to pathogen attacks (Wei & Shirsat, 2006). The mechanism by which cross-linking of extensins through tyrosine residues strengthens the cell walls has also been proposed (Cannon et al., 2008). This is further supported by our observation of extensins in the cell corners of parenchyma tissue in *siPsGALS3* plants.

The precise function of galactan in the cell wall, especially how it affects cell extensibility, has not been satisfactorily elucidated. It may act by separating pectin and other cell wall component chains, thereby altering pectin gelation properties (Willats et al., 2006; Gao et al., 2023). The observed consequent changes in the extensin epitope in the present study indicate the presence of a cell wall-sensing pathway that monitors galactan levels directly or the effects of changes in galactan content *in muro*. Additionally, the loss of galactan seems to trigger a potential compensatory mechanism involving extensins in both pea and Arabidopsis. Numerous cell wall-associated kinases and integrity-sensing systems have been shown to sense pectin-mediated cell wall homeostasis (Gigli-Bisceglia et al., 2020; Moussu et al., 2023a;ßling et al., 2024). However, no galactan-specific receptor-like kinase has yet been identified. In this case, rather than a general cell wall homeostasis surveillance or stress-sensing mechanism, a specific mechanism might be involved.

In conclusion, by using a model other than Arabidopsis, we provided further evidence that galactan is indispensable for cell wall function and plant development. More extensive molecular and genetic studies on peas should now be facilitated by the availability of the pea draft genome (Liu et al., 2024). However, more molecular data on the interactions among various cell wall components *in muro* are needed to accurately understand the mechanisms of all cell wall processes.

Material and methods

Plant material and growth conditions

Pisum sativum cv. Kelvedon Wonder seeds (Frøbutikken, Denmark) were sterilized with absolute hypochlorite for 3 minutes by shaking, rinsed in sterile water at least five times, and left in the last rinse for 1 hour. They were then placed on wet tissue inside a sterilized plastic box in the dark at room temperature for five days to germinate. Seedlings that germinated synchronously with roots around 3–4 cm were transferred to soil (Pindstrup Mosebrug A/S, Denmark), with one seedling per 11 cm pot. Plants were grown at 22°C/20°C under a 16-hour/8-hour day/night cycle in a growth chamber illuminated with fluorescent light (200 µmol m-2s-1).

Auxin-induced stem curvature

The setup has been described by Velasquez et al. (2021). Three-week-old pea plants were decapitated at the second internode counting from the tip. Lanolin paste containing indole-3-acetic acid (IAA, Sigma-Aldrich) at 10mg/g was applied to one side of the stem of the second internode. The wound surface introduced by decapitation was covered by lanolin without IAA for protection from dehydration. Curvature or straight stems were harvested after 3 days of treatment. The curvature was dissected from the middle to separate the longer and shorter sides, and a pull of three curvatures was used for further analysis of cell wall composition.

Preparation of alcohol insoluble residues

Plant materials were first homogenized using TissueLyser (Sigma-Aldrich) with a metal bead at maximum speed. Alcohol-insoluble residue (AIR) was prepared following sequential extraction with 70% ethanol, methanol: chloroform at 1:1 (v/v), and absolute acetone. Each solvent was added to the samples at 6:1 (v/v) and mixed thoroughly by vortexing. Each extraction lasted 10 minutes with shaking, then the samples were centrifuged at 14000 rpm for 10 minutes. The supernatant was discarded, and the samples were left to dry in the fume hood. AIR from pea stem curvature was used in monosaccharide analysis and epitope detection chromatography. The AIR from a virus-silenced pea plant stem was used in comprehensive microarray polymer profiling (MAPP).

Microarray polymer profiling

MAPP analysis was conducted as previously described. AIR samples (fresh samples for auxin-induced curvature) were extracted sequentially with two solvents: 50 mM CDTA and 4M NaOH with 1% (v/v) NaBH4 at 30:1 (µl/mg). After 2 hours of extraction with shaking, followed by centrifugation at 4000 rpm, supernatants were spotted onto nitrocellulose membranes in four replicates and four dilutions at ratios of 1:2, 1:6, 1:18, and 1:54 [v/v]. The microarray was probed with cell wall-specific probes, and the binding intensity was quantified as MAPP data. Data were presented in two formats: a heat map and a line chart. The heat map displayed the relative intensity of different polysaccharides across the full probe list by applying overall scaling—the maximum signal observed was set as 100, and other signals were scaled proportionally. A fold change heat map for the auxin-induced curvature experiment was generated by

dividing the signal from the longer or shorter side of the curvature by that of the straight stem. If the value was less than 1, it was transformed using the formula: = -1/value. This resulted in a negative value representing downregulation. The line chart was created by plotting individual scaled MAPP data for each probe, with one probe consistently showing a value of 100.

Monosaccharide composition analysis

Monosaccharide analysis was carried out as previously described. 1 mg of AIR sample was hydrolyzed in 2 M trifluoroacetic acid (TFA) for 1 h at 120°C and dried using vacuum spin to remove TFA. Residuals resolved in H_2O and applied to ICS 3000 (Dionex) with a PA20 column performing high-performance anion-exchange chromatography with pulsed amperometric detection (HPAEC-PAD). Monosaccharide standards included L-Fuc, L–Rha, L-Ara, D-Gal, D-Glc, D-Xyl, D-GalUA, and D-GlcA (Sigma-Aldrich).

Epitope detection chromatography

Epitope detection chromatography (EDC) was carried out as previously described (Cornuault et al. 2014). AIR samples were extracted using CDTA. 50 µl of the extraction was diluted in 2.5 ml H2O and eluted through a 1 ml Hi-Trap ANX FF anion-exchange column (GE Healthcare) with Na_2CO_3 buffer. 100 µl of fraction aliquots were incubated overnight at 4°C in a microtitre plate and probed with cell wall-specific probes. The absorbance intensity was determined at 450 nm using an ELISA plate reader (BioTek).

Immunolocalization

Transverse sections were prepared from approximately 1 cm stem segments embedded in 8% agarose and sectioned using a Leica VT1000s vibratome. The stem segments were preserved in 70% ethanol and then rehydrated in PBS before being embedded in agarose. The blocks were sectioned to generate 200 µm-thin slices. The sections were collected in a 24-well microplate. They were blocked with 5% skimmed milk powder in PBS for 30 minutes and then incubated with primary antibodies at a 1:10 dilution for 1 hour. The secondary antibody, goat anti-rat IgG AlexaFluor 488 (Invitrogen), was prepared at a 1:500 dilution and incubated for 1 hour. After three washes with PBS, sections were stained with Calcofluor White (Sigma-Aldrich) at 0.1 mg/ml for 10 minutes for counterstaining. Immunolabeled sections were mounted in CitiFluor (Agar Scientific) before observation.

Laser Scanning Confocal Microscopy

Imaging was performed using a Leica SP5 confocal microscope with UV diode (405 nm) and Argon (488 nm) lasers. Imaging of the longitudinal section was performed using an Olympus BX61 microscope equipped with epifluorescence irradiation. Images were processed with the GIMP2 software only to enhance the contrast and brightness. All scans were treated equally.

DNA cloning

RNA was extracted from 100 mg of leaf tissue (SpectrumTM Plant total RNA kit, Sigma Aldrich) and used as a template for cDNA synthesis (Superscript supermix, Thermo-Fisher Scientific). VIGS construct pCAPE2-PsGALS3 was constructed by PCR amplification of a 463 bp fragment of PsGALS3 with primers

PsGALS3-C-F and PsGALS3-C-R and USER cloning (Nour-Eldin et al., 2010) into pCAPE2-USER. pCAPE2-USER was constructed by replacing the GFP coding region of pCAPE2-GFP (Constantin et al., 2004) with the sequence GCTGAGGCAATTTAAATACCCTCAGC. pCAPE2-USER was linearised with *Swa*I (New England Biolabs) and overhangs generated by *N.BbvC* IB (New England Biolabs). For primers used see Table S1.

Virus-induced gene silencing

Virus-induced gene silencing was performed as described earlier (Grønlund et al. 2010). The pea early browning virus (PEVB) system uses binary vectors derived from pCAMBIA 1300, named pCAPE1 and pCAPE2. These vectors were separately transformed into the Agrobacterium strain GV3101 and cultured. The bacteria were collected by centrifuging at 3500g once the culture reached an optical density of 1.2–1.5 at OD550, then resuspended in infiltration buffer (10 mM NaCl, 1.75 mM CaCl2, 100 µM acetosyringone). The cultures containing pCAPE1 and pCAPE2 were mixed 1:1. This mixture was infiltrated into the abaxial side of leaves of 2-week-old pea plants using a 1 ml syringe. pCAPE2 containing GFP was used as a control. Ten days post-infiltration, pea plants were decapitated at the nodules formed after infiltration. New shoots emerged from the bottom of the plants. Samples for analysis were collected three weeks after decapitation. Photographs of VIGS-silenced pea plants were taken with a Canon EOS 20D camera equipped with an EFS 60mm lens. Internode length and Arabidopsis root length were measured using ImageJ software (https://imagej.nih.gov/ij/). Internodes were numbered from the most apical (1) to the basal (5).

PsGALS3 expression analysis

For semi-quantitative PCR (Semi-qRT-PCR), RNA was extracted from 100 mg of leaf tissue (SpectrumTM Plant total RNA kit, Sigma Aldrich). 500ng RNA was used as a template for cDNA synthesis (Superscript supermix). For semi-qRT-PCR, a 188 bp fragment of PsGALS3 was amplified with primers PsGALS3-sqF and PsGALS3-sqR, and a 573 bp fragment of β-tubulin cDNA (accession no. NM_001427110.1) with primers TUB-F1 and TUB-R1. PsGALS3 Semi-qRT-PCR primers were predicted to span one intron based on the corresponding *Arabidopsis* gDNA sequences At5g44670 and At4g20170, while tubulin Semi-qRT-PCR primers span two introns in pea gDNA (X54844). PCR conditions were optimised, and were run for 30 cycles of 30 sec at 94°C, 30 sec at 61°C, and 40 sec at 72°C. PCR products were loaded into the same gel by first loading 14µl of 188 bp *PsGALS3* fragment, electrophoresing for 5 min, followed by loading 14 µl of 573 bp tubulin fragment. For RT-qPCR on silence plants, RNA was extracted from 100 mg of leaf tissue (SpectrumTM Plant total RNA kit). 3.5µg RNA was treated with DNA-free Turbo (Ambion), and 850 DNAse-treated RNA was used as template for cDNA synthesis (iscriptTM cDNA synthesis kit, Bio-Rad). Transcription factor 2a (TFIIA; accession no. XM_051028068.1) was selected as a household reference and amplified with primers TFIIA-F1 and TFIIA-R1. Analysis of expression in organs: Total RNA was extracted from three-day-old seedlings and various organs, namely young leaves, old leaves, internodes I and II, flowers (without sepals), young pods (without ovules), ovules, and tendrils using the Quick-RNA™ Plant Miniprep Kit (Zymo Research, USA) with DNase treatment. First-strand cDNA was synthesized from

1 µg of total RNA from each organ using the RevertAid First Strand cDNA Synthesis Kit (Thermo Fisher Scientific, USA) with a mixture of oligo(dT) and random primers.

Quantitative real-time PCR (qRT–PCR) was performed using the FastStart Essential DNA Green Master Mix (Roche) on a LightCycler® 96 system. The reference genes phosphoprotein phosphatase 2A (PP2A; accession no. NM_001427333.1),TFIIA, and β-tubulin were selected based on their reported expression stability (Die et al., 2010; Knopkiewicz and Wojtaszek, 2018). Amplification specificity was confirmed by melt-curve analysis. Ct values from three technical replicates were averaged for each of two biological replicates. Relative expression levels of *PsGALS3* were calculated using an efficiency-corrected method ($RQ = E^{-Ct}$, where RQ represents relative quantities and E is the PCR amplification efficiency), and normalised to the geometric mean of the reference genes. Standard error (SE) was calculated from efficiency-corrected normalised expression values obtained from biological replicates. For primers used see Table S1.

Declarations

Author Contribution

XG conducted auxin physiological and most cell wall compositional analyses; XG and IEJ conducted the VIGS experiments; AK conducted expression analysis and bioinformatics; and JH conducted monosaccharide analysis. XG, WW, PU, and JM contributed to conceptualization and wrote the first draft of the manuscript.

Acknowledgement

We would like to thank Professor Emeritus Paul Knox for his generous help with antibodies and microscopy, and Dr. Valérie Cornuault for her technical support with EDC and data analysis.

References

1. Aryal B, Jonsson K, Baral A, Sancho-Andres G, Routier-Kierzkowska AL, Kierzkowski D, Bhalerao RP (2020) Interplay between cell wall and auxin mediates the control of differential cell elongation during apical hook development. Curr Biol 30:1733–1739e3
2. Amos RA, Mohnen D (2019) Critical review of plant cell wall matrix polysaccharide glycosyltransferase activities verified by heterologous protein expression. Front Plant Sci 10:915
3. Anderson CT, Pelloux J (2025) The dynamics, degradation, and afterlives of pectins: influences on cell wall assembly and structure, plant development and physiology, agronomy, and biotechnology. Annu Rev Plant Biol 76:85–113
4. Bakshani CR, Sangta J, Sommano S, Willats WGT (2023) Microarray polymer profiling (MAPP) for high-throughput glycan analysis. J Vis Exp 199:e65443

5. Bret-Harte MS, Talbott LD (1993) Changes in composition of the outer epidermal cell wall of pea stems during auxin-induced growth. Planta 190:369–378
6. Cannon MC, Terneus K, Hall Q, Tan L, Wang Y, Wegenhart BL, Chen L, Lamport DTA, Chen Y, Kieliszewski MJ (2008) Self-assembly of the plant cell wall requires an extensin scaffold. Proc Natl Acad Sci USA 105:2226–2231
7. Catalá C, Rose JKC, Bennett AB (1997) Auxin regulation and spatial localization of an endo-1,4-β-D-glucanase and a xyloglucan endotransglycosylase in expanding tomato hypocotyls. Plant J 12:417–426
8. Coenen GJ, Bakx EJ, Verhoef RP, Schols HA, Voragen AGJ (2007) Identification of the connecting linkage between homo- or xylogalacturonan and rhamnogalacturonan type I. Carbohydr Polym 70:224–235
9. Constantin GD, Krath BN, MacFarlane SA, Nicolaisen M, Johansen IE, Lund OS (2004) Virus-induced gene silencing as a tool for functional genomics in a legume species. Plant J 40:622–631
10. Cosgrove DJ (2024) Structure and growth of plant cell walls. Nat Rev Mol Cell Biol 25:340–358
11. Cornuault V, Manfield IW, Ralet MC, Knox JP (2014) Epitope detection chromatography: a method to dissect the structural heterogeneity and inter-connections of plant cell-wall matrix glycans. Plant J 78:715–722
12. Die JV, Román B, Nadal S, González-Verdejo CI (2010) Evaluation of candidate reference genes for expression studies in Pisum sativum under different experimental conditions. Planta 232:145–153
13. Du M, Spalding EP, Gray WM (2020) Rapid auxin-mediated cell expansion. Annu Rev Plant Biol 71:379–402
14. Ebert B, Birdseye D, Liwanag AJM, Laursen T, Rennie EA, Guo X, Catena M, Rautengarten C, Stonebloom SH, Gluza P, Pidatala VR, Andersen MCF, Cheetamun R, Mortimer JC, Heazlewood JL, Bacic A, Clausen MH, Willats WGT, Scheller HV (2018) The three members of the Arabidopsis glycosyltransferase family 92 are functional β-1,4-galactan synthases. Plant Cell Physiol 59:2624–2636
15. Fangel JU, Sørensen KM, Jacobsen N, Mravec J, Ahl LI, Bakshani C, Mikkelsen MD, Engelsen SB, Willats WGT, Ulvskov P (2024) The legacy of terrestrial plant evolution on cell wall fine structure. Plant Cell Environ 47:1238–1254
16. Fendrych M, Leung J, Friml J (2016) TIR1/AFB-Aux/IAA auxin perception mediates rapid cell wall acidification and growth of Arabidopsis hypocotyls. eLife 5:e19048
17. Geshi N, Pauly M, Ulvskov P Solubilization of galactosyltransferase that synthesizes 1,4-β-galactan side chains in pectic rhamnogalacturonan I. Physiol Plant 114:540–548., Gao Y, Lipton AS, Munson CR, Ma Y, Johnson KL, Murray DT, Scheller HV, Mortimer JC (2002) (2023) Elongated galactan side chains mediate cellulose–pectin interactions in engineered Arabidopsis secondary cell walls. Plant J 115:529–545
18. Geitmann A (2023) Plant cell walls: research milestones and conceptual insights. CRC, Boca Raton

19. Gigli-Bisceglia N, Engelsdorf T, Hamann T (2020) Plant cell wall integrity maintenance in model plants and crop species. Cell Mol Life Sci 77:2049–2077
20. Gilkes NR, Hall MA (1977) The hormonal control of cell wall turnover in Pisum sativum L. New Phytol 78:1–15
21. Goldberg R, Morvan C, Hervé du Penhoat C, Michon V (1989) Structure and properties of acidic polysaccharides from mung bean hypocotyls. Plant Cell Physiol 30:163–173
22. Grønlund M, Olsen A, Johansen EI, Jakobsen I (2010) Using virus-induced gene silencing to study the arbuscular mycorrhizal symbiosis in Pisum sativum. Plant Methods 6:28
23. Goubet F, Morvan C (1994) Synthesis of cell wall galactans from flax (Linum usitatissimum L.) suspension-cultured cells. Plant Cell Physiol 35:719–727. https://doi.org/10.1093/oxfordjournals.pcp.a078649
24. Hager A, Menzel H, Krauss A (1971) Primary action of auxin in elongation growth. Planta 100:47–75
25. Houston K, Tucker MR, Chowdhury J, Shirley N, Little A (2016) The plant cell wall: a complex and dynamic structure revealed by gene responses under stress. Front Plant Sci 7:984
26. Jones L, Seymour GB, Knox JP (1997) Localization of pectic galactan in tomato cell walls using a monoclonal antibody specific to (1→4)-β-D-galactan. Plant Physiol 113:1405–1412
27. Jonsson K, Routier-Kierzkowska AL, Bhalerao RP (2025) The asymmetry engine: how plants harness asymmetries to shape their bodies. New Phytol 245:2422–2427
28. Kumar V, Yadav S, Heymans A, Robert S (2025) Shape of cell: an auxin and cell wall duet. Physiol Plant 177:e70294
29. Knopkiewicz M, Wojtaszek P (2019) Validation of reference genes for qPCR analysis in pea lines with different lodging susceptibility. Ann Appl Biol 174:86–91
30. Labavitch JM, Ray PM (1974) Turnover of cell-wall polysaccharides in elongating pea stem segments. Plant Physiol 53:669–673
31. Laursen T, Stonebloom SH, Pidatala VR, Birdseye DS, Clausen MH, Mortimer JC, Scheller HV (2018) Bifunctional glycosyltransferases catalyze both extension and termination of pectic galactan oligosaccharides. Plant J 94:340–351
32. Lee Y, Ayeh KO, Ambrose M, Hvoslef-Eide AK (2016) Immunolocalization of pectic polysaccharides during abscission in pea seeds. BMC Res Notes 9:427
33. Liwanag AJM, Ebert B, Verhertbruggen Y, Rennie EA, Rautengarten C, Oikawa A, Andersen MCF, Clausen MH, Scheller HV (2012) GALS1 is a β-1,4-galactan galactosyltransferase in Arabidopsis. Plant Cell 24:5024–5036
34. Liu N, Lyu X, Zhang X, Zhang G, Zhang Z, Guan X, Chen X, Yang X, Feng Z, Gao Q, Shi W, Deng Y, Sheng K, Ou J, Zhu Y, Wang B, Bu Y, Zhang M, Zhang L, Zhao T, Gong Y (2024) Reference genome and population genomics of peas. Nat Genet 56:1964–1974
35. Marcus SE, Verhertbruggen Y, Hervé C, Ordaz-Ortiz JJ, Farkas V, Pedersen HL, Willats WGT, Knox JP (2008) Pectic homogalacturonan masks xyloglucan epitopes in plant cell walls. BMC Plant Biol 8:60

36. Matchett WH, Nance JF (1962) Cell wall breakdown and growth in pea seedling stems. Am J Bot 49:311–319
37. McCartney L, Ormerod AP, Gidley MJ, Knox JP (2000) Regulation of pectic (1→4)-β-D-galactan in developing pea cotyledons. Plant J 22:105–113
38. McCartney L, Steele-King CG, Jordan E, Knox JP (2003) Pectic (1→4)-β-D-galactan marks acceleration of cell elongation in Arabidopsis roots. Plant J 33:447–454
39. Moller I, Sorensen I, Bernal AJ, Blaukopf C, Lee K, Obro J, Pettolino F, Roberts A, Mikkelsen JD, Knox JP, Bacic A, Willats WGT (2007) High-throughput mapping of cell-wall polymers using microarrays. Plant J 50:1118–1128
40. Moneo-Sánchez M, Alonso-Chico A, Knox JP, Dopico B, Labrador E, Martín I (2019) β-(1,4)-Galactan remodelling affects xyloglucan structure during elongation. Planta 249:351–362
41. Moore JP, Fangel JU, Willats WGT, Vivier MA (2014) Galactan, extensin and AGP epitopes differentiate grape ripening stages. Ann Bot 114:1279–1294
42. Moussu S, Ingram G (2023) The extensin enigma. Cell Surf 9:100094
43. Moussu S et al (2023) Plant cell wall patterning and expansion mediated by protein–peptide–polysaccharide interaction. Science 382:719–725
44. Nour-Eldin HH, Geu-Flores F, Halkier BA (2010) USER cloning and USER fusion: the ideal cloning techniques for small and big laboratories. Methods Mol Biol 643:185–200
45. Paniagua C, Posé S, Morris VJ, Kirby AR, Quesada MA, Mercado JA (2014) Fruit softening and pectin disassembly. Ann Bot 114:1375–1383
46. Petrova A, Sibgatullina G, Gorshkova T, Kozlova L (2022) Dynamics of cell wall polysaccharides during the elongation growth of rye primary roots. Planta 255:108
47. Prabhakar PK, Pereira JH, Taujale R, Shao W, Bharadwaj VS, Chapla D, Yang JY, Bomble YJ, Moremen KW, Kannan N, Hammel M, Adams PD, Scheller HV, Urbanowicz BR (2023) Structural insight into a modular β-1,4-galactan synthase. Nat Plants 9:486–500
48. Rößling AK, Dünser K, Liu C, Lauw S, Rodriguez-Franco M, Kalmbach L, Barbez E, Kleine-Vehn J (2024) Pectin methylesterase activity is required for RALF1 signaling output. eLife 13:RP96943
49. Saito F, Suyama A, Oka T, Yoko-o T, Matsuoka K, Jigami Y, Shimma YI (2014) Novel peptidyl serine α-galactosyltransferases in plants. J Biol Chem 289:20405–20420
50. Sauer M, Balla J, Luschnig C, Wisniewska J, Reinöhl V, Friml J, Benková E (2006) Canalization of auxin flow by Aux/IAA–ARF feedback regulation. Genes Dev 20:2902–2911
51. Tan L, Eberhard S, Pattathil S, Warder C, Glushka J, Yuan C, Hao Z, Zhu X, Avci U, Miller JS, Baldwin D, Pham C, Orlando R, Darvill A, Hahn MG, Kieliszewski MJ, Mohnen D (2013) An Arabidopsis cell wall proteoglycan covalently links pectin and arabinoxylan to an AGP. Plant Cell 25:270–287
52. Ulvskov P, Wium H, Bruce D, Jørgensen B, Qvist KB, Skjøt M, Hepworth D, Borkhardt B, Sørensen SO (2005) Biophysical consequences of remodeling the neutral side chains of rhamnogalacturonan I in tubers of transgenic potatoes. Planta 220:609–620

53. Velasquez SM, Guo X, Gallemi M, Aryal B, Venhuizen P, Barbez E, Dünser KA, Darino M, Pěnčík A, Novák O, Kalyna M, Mouille G, Benková E, Bhalerao RP, Mravec J, Kleine-Vehn J (2021) Xyloglucan remodeling defines auxin-dependent differential tissue expansion. Int J Mol Sci 22:9222
54. Velasquez SM, Ricardi MM, Dorosz JG, Fernandez PV, Nadra AD, Pol-Fachin L, Egelund J, Gille S, Harholt J, Ciancia M, Verli H, Pauly M, Bacic A, Olsen CE, Ulvskov P, Petersen BL, Somerville C, Iusem ND, Estevez JM (2011) O-glycosylated cell wall proteins are essential for root hair growth. Science 332:1401–1403
55. Willats WGT, Steele-King CG, Marcus SE, Knox JP (1999) Side chains of pectic polysaccharides are regulated during cell proliferation and differentiation. Plant J 20:619–628
56. Willats WGT, Knox JP, Mikkelsen JD (2006) Pectin: new insights into an old polymer are starting to gel. Trends Food Sci Technol 17:97–104
57. Wilson MH, Holman TJ, Sørensen I, Cancho-Sanchez E, Wells DM, Swarup R, Knox JP, Willats WGT, Ubeda-Tomás S, Holdsworth M, Bennett MJ, Vissenberg K, Hodgman TC (2015) Multi-omics analysis identifies genes mediating cell wall extension in Arabidopsis roots. Front Cell Dev Biol 3:10
58. Yan J, Liu Y, Yang L, He H, Huang Y, Fang L, Scheller HV, Jiang M, Zhang A (2021) Cell wall β-1,4-galactan regulated by BPC1/BPC2–GALS1 aggravates salt sensitivity. Mol Plant 14:411–425
59. Zhang L, Gao C, Gao Y, Yang H, Jia M, Wang X, Zhang B, Zhou Y (2025) New insights into plant cell wall functions. J Genet Genomics 52:1308–1324

Figures

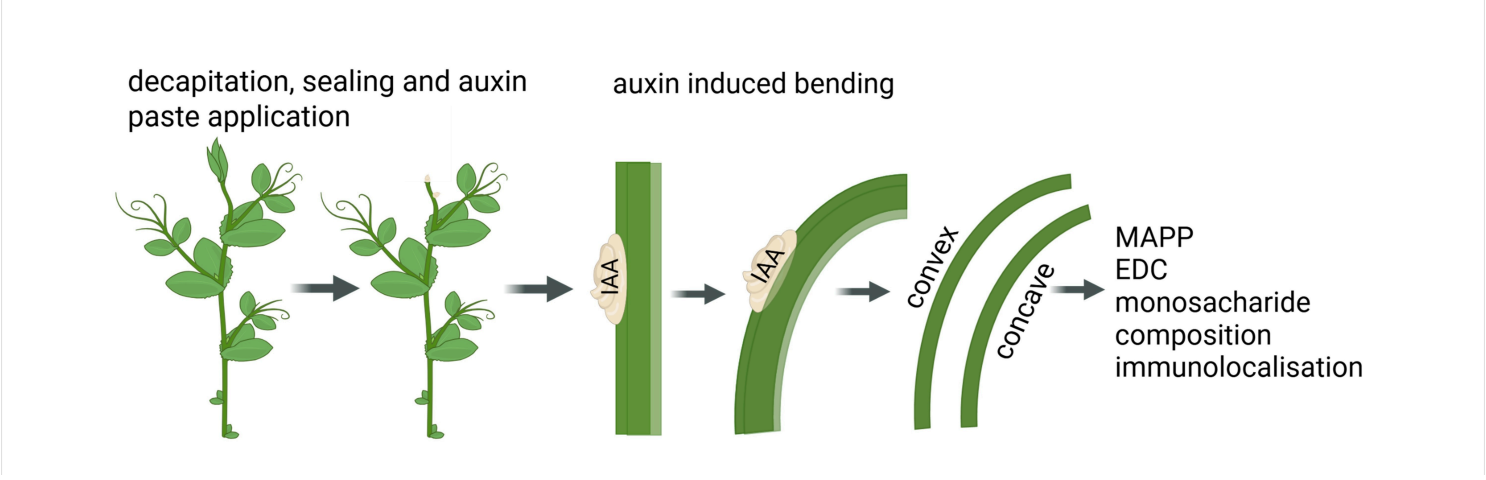

Figure 1

Diagram of auxin-induced bending in pea stems. The pea plants were decapitated, and the wound was sealed with pure lanolin. The lanolin paste containing IAA was applied laterally. The convex and concave sites were dissected and analysed using various methods.

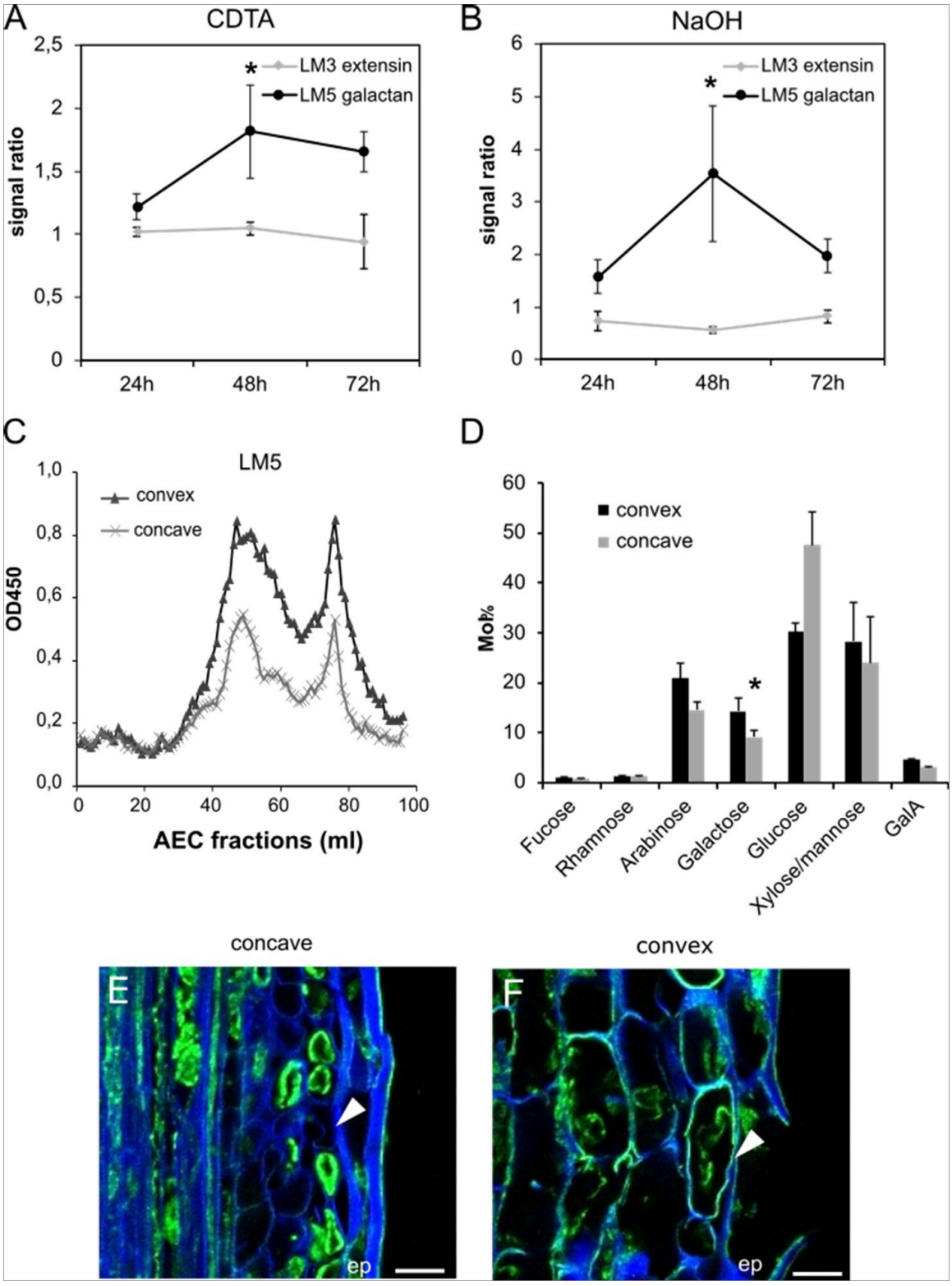

Figure 2

Changes in galactan content in auxin-induced curvature in pea stems. **(A,B)** Relative comparison between the concave (shorter) and convex (longer) parts of auxin-induced curvature. LM5 and LM3 binding on extracts from the opposing sides, showing relative amounts of cell wall epitopes detected by specific monoclonal antibodies on different parts of curvature. (**A**) CDTA extraction is rich in pectic and easily extractable epitopes, while (**B**) NaOH extraction contains abundant hemicellulose and tightly

bound polymers. Values are means of eight biological replicates. **(C)** Analysis of the extracts with EDC. The chromatogram for LM5 epitope detection indicates similar structural features of the galactan on opposite sides. The experiment was performed with three replicas with comparable results. **(D)**Monosaccharide composition analysis of AIR derived from curvature confirms an increase in galactose on the convex side compared to the concave side (mean ± SD of three biological replicates; *P < 0.05, t-test). (**E, F**) Immunolocalization of LM5 epitopes in the wax sections through concave and convex sites of the IAA-stimulated stem curvature. Upregulation of the LM5 epitopes (green, arrowheads) is visible in the cell wall of cortical tissue in the convex site. Note the more expanded cortical cells. The cell wall is counterstained with Calcofluor White (blue signal). Scale bars = 20 µM.

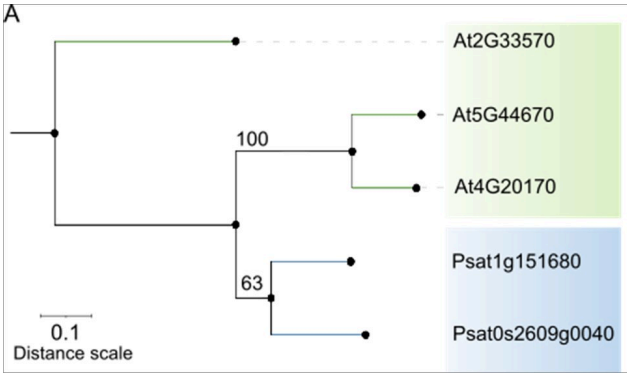

B

	At2G33570	At5G44670	At4G20170	Psat1g151680	Psat0s2609g0040
At2G33570	100	45.81	45.3	48.15	47.36
At5G44670	45.81	100	77.49	60.67	61.6
At4G20170	45.3	77.49	100	61.84	61.24
Psat1g151680	48.15	60.67	61.84	100	71.6
Psat0s2609g0040	47.36	61.6	61.24	71.6	100

Figure 3

Phylogenetic tree and heat map of sequence identity for GT92 GALS proteins. **(A)** The Maximum likelihood tree of Arabidopsis At2G33570 (AtGALS1), At5G44670 (AtGALS2), At4G20170 (AtGALS3), and pea homologs Psat1g151680 (PsGALS3) and Psat0s2609g0040 (PsGALS2). The analysis uses the JTT substitution model, and bootstrap values of 50% or higher are shown. The tree is scaled, with branch lengths indicating substitutions per site. **(B)** Pairwise amino acid sequence identities (%) were calculated for Arabidopsis At2G33570 (AtGALS1), At5G44670 (AtGALS2), At4G20170 (AtGALS3), and pea homologs Psat1g151680 (PsGALS3) and Psat0s2609g0040 (PsGALS2). Darker green shades indicate higher identity scores, and lighter green shades represent lower scores, transitioning to white. The diagonal values (100%) represent self-identity.

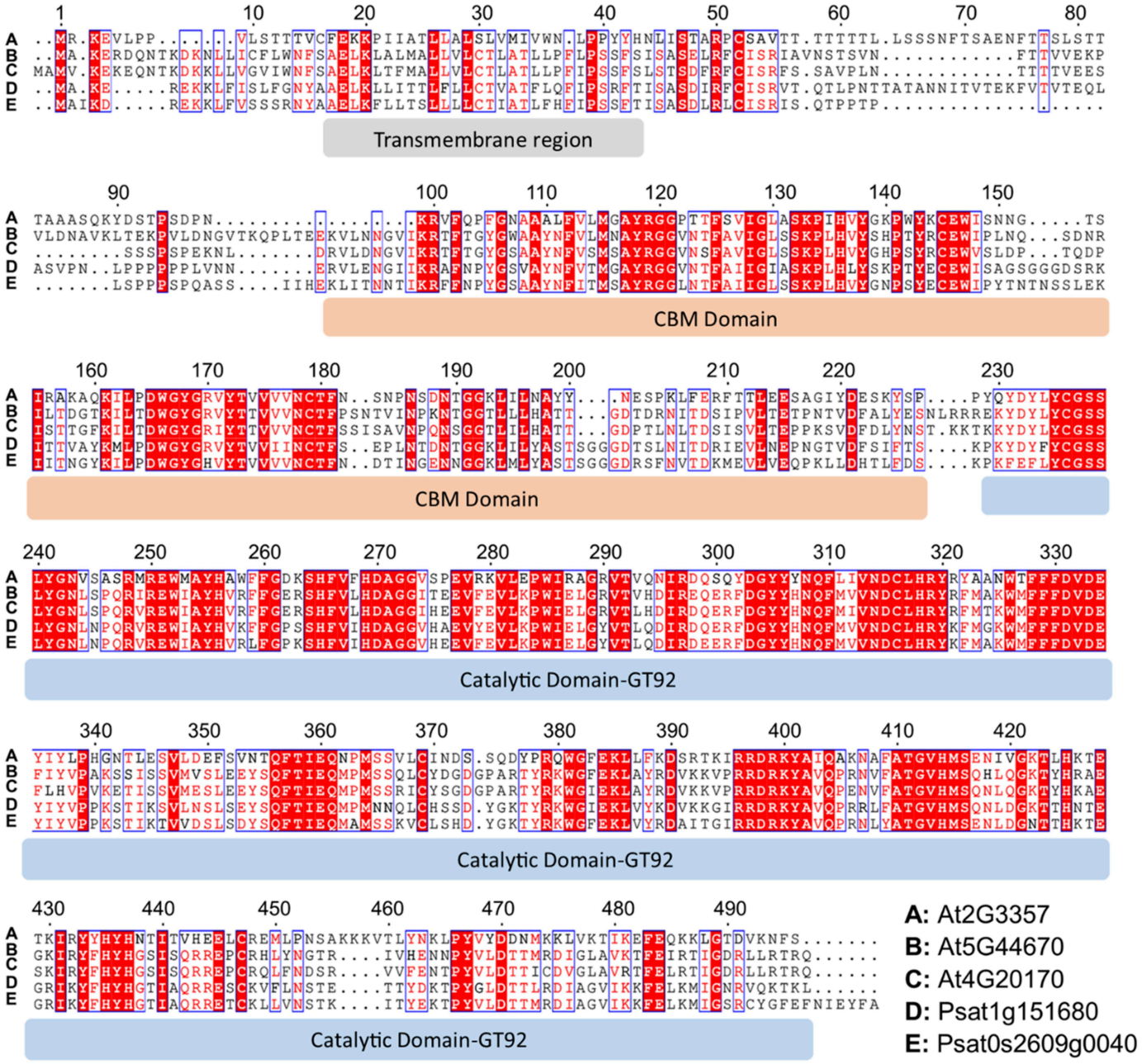

Figure 4

Multiple sequence alignment of the GT92 GALS proteins. Sequence similarity is shown by a white-to-red gradient background, with dark red indicating residues with a global similarity of ≥0.7. Identical residues are highlighted in red font. Highly conserved positions with strong local agreement are marked by blue-framed boxes. The predicted transmembrane segment is indicated by a grey bar. Domain annotations were obtained from Prabhakar et al. (2023) and CATH superfamily classifications: the N-terminal β-sandwich/Jelly-roll fold (CATH 2.60.40) is shown in brown, and the C-terminal GT-A fold catalytic domain (CATH 3.90.550) is shown in light blue.

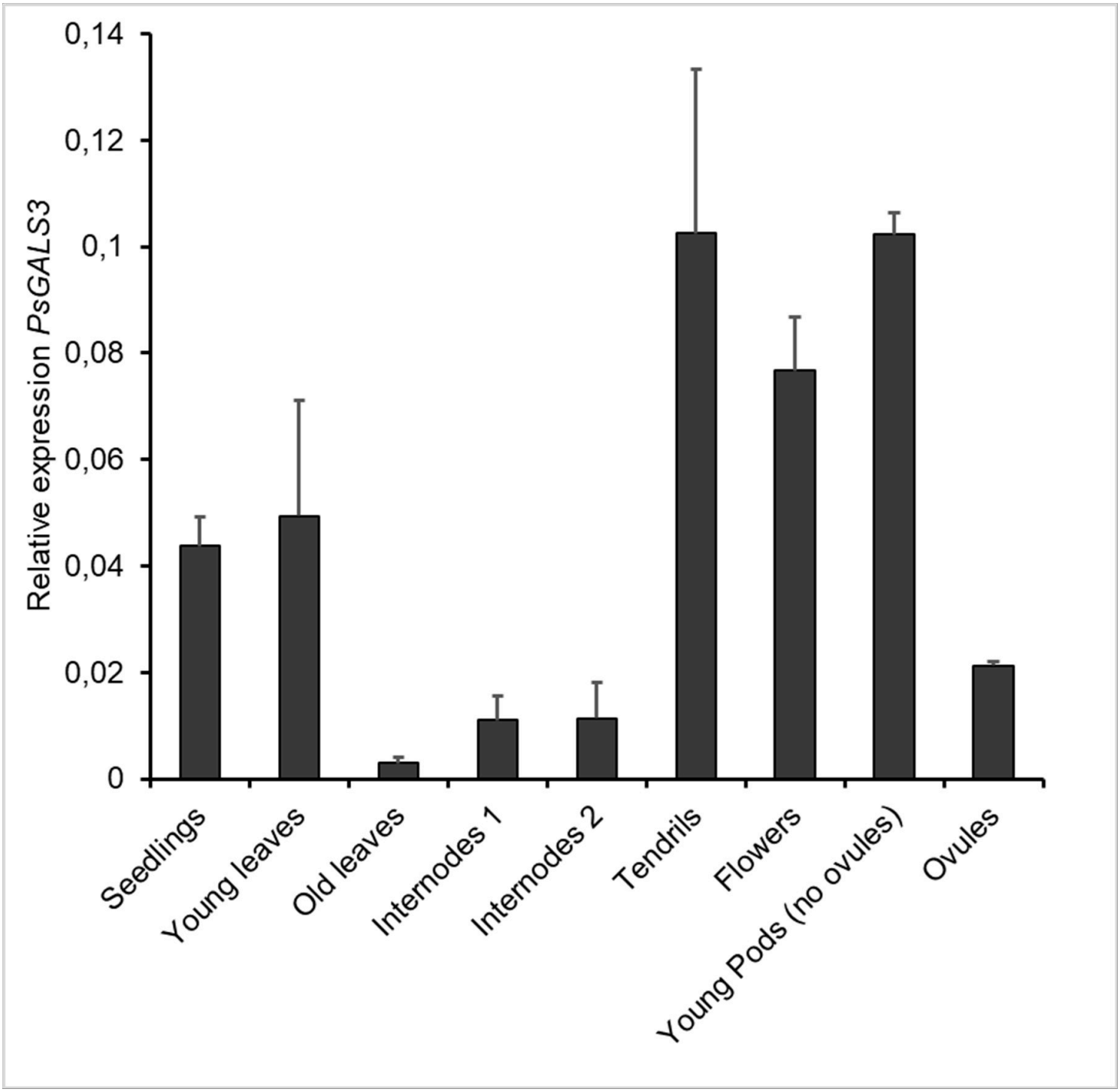

Figure 5

Expression analysis of *PsGALS3*. RT-qPCR analysis of 8 aerial organs, including whole seedlings. The expression against two reference genes. Bars represent mean efficiency-corrected normalised expression, and error bars indicate SE calculated from biological replicates.

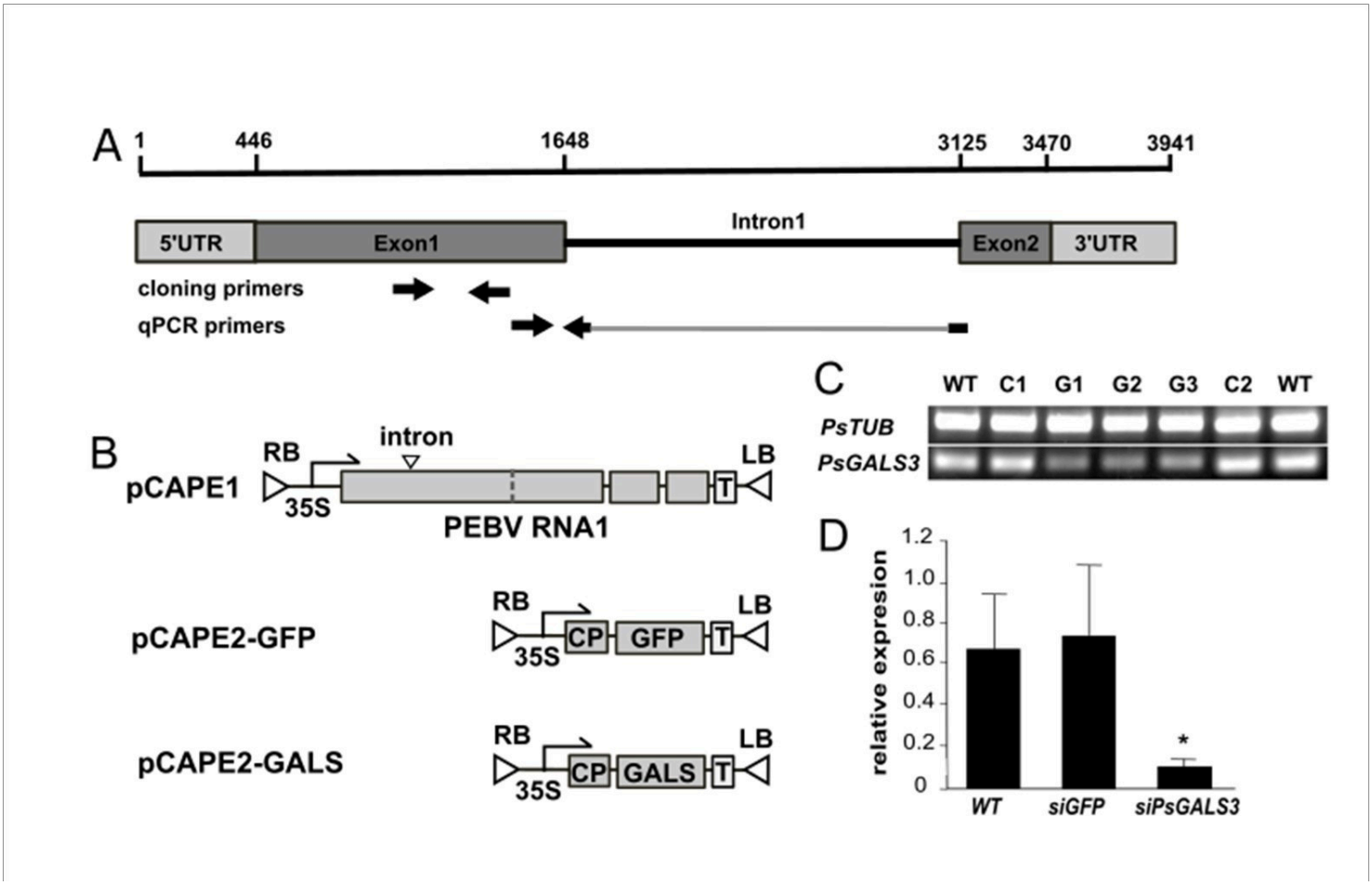

Figure 6

VIGS vector construction and determination of *PsGALS3* silencing efficiency (**A**) The scheme of *the PsGALS3* gene with depicted exons and an intron, and primers used for cloning of VIGS constructs and PCR. (**B**) *Pea early browning virus* (PEVB) RNA1 and RNA2 were inserted into pCAPE1 and pCAPE2, respectively. pCAPE2 carried genes encoding the virus coating protein (CP) and *PsGALS fragment. GFP* insertion was used as a virus (vector) control (pCAPE-GFP; *siGFP*). (**C**) Semiquantitative PCR analysis of silencing efficiency with β-tubulin as a housekeeping control (top panel) showed a downregulation of *PsGALS2* (lower panel) in *siPsGALS* (G1, G2, G3) compared to WT (WT1, WT2) and control *siGFP* (C1, C2) plants. (**D**) Real-time qPCR showed a significant reduction in *PsGALS2*mRNA levels in the *siPsGAL3* plant. The level of expression was calculated relative to the TFII gene. (mean ± SD of three biological replicates; *P < 0.05, t test).

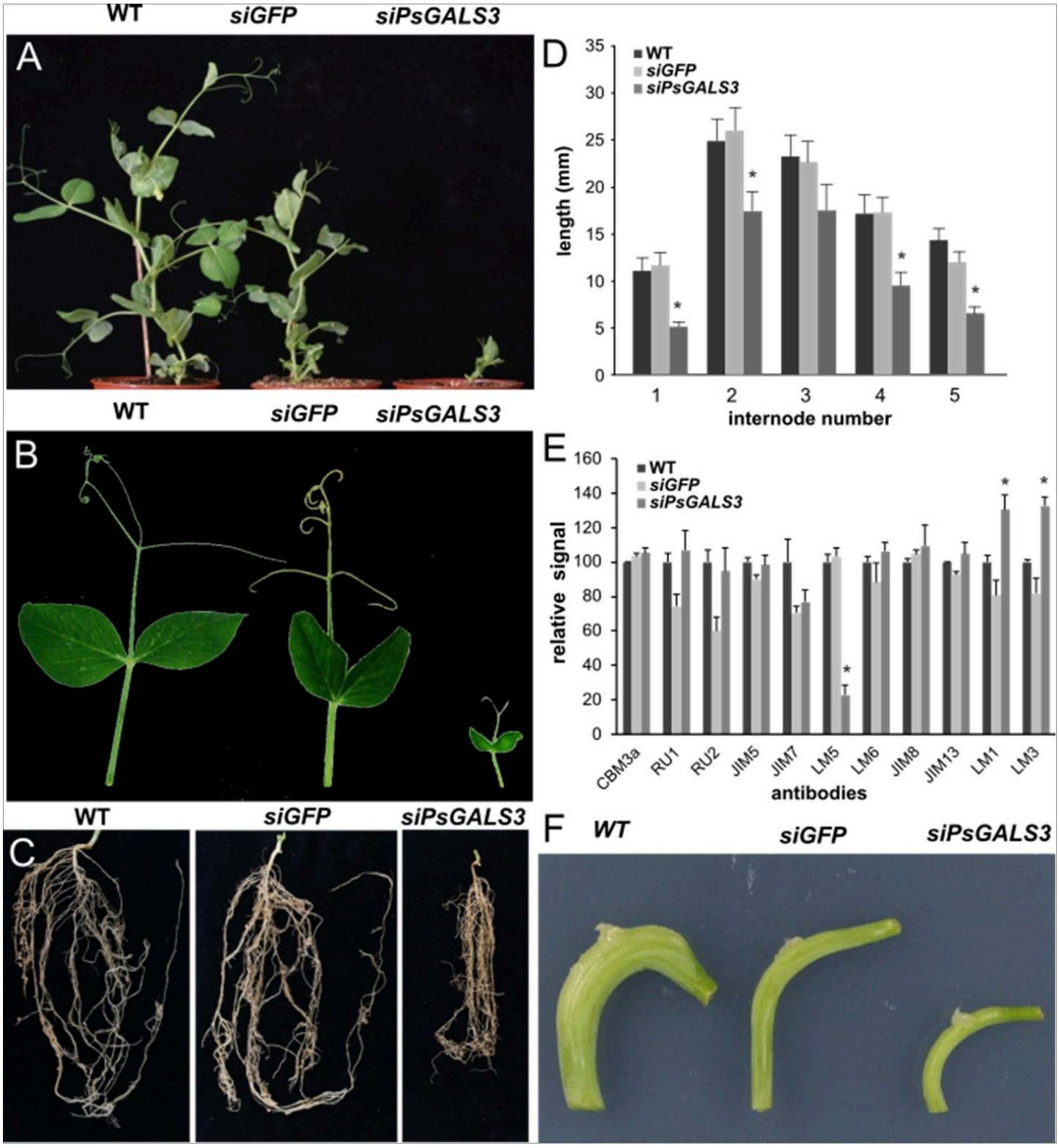

Figure 7

Phenotypes of *PsGALS3*-silenced plants. (**A**) Phenotypes of pea plants three weeks after virus inoculation. The *PsGALS3*-silenced plant showed a dwarf phenotype compared to the *siGFP* control and wild type. (**B**) *siPsGALS3* plants showed defects in aerial organ expansion and (**C**) reduced root system. (**D**) Quantification of internode length. *PsGALS3*-silenced plants significantly reduced the length of internodes (mean ± SEM of 12 biological replicates; *P < 0.05; t-test). (**E**) MAPP analysis of *siPsGALS3*

plants. Profiling showed the relative abundance of solvent-extractable cell wall epitopes. The LM5 signal was decreased significantly in the silenced plant, while extensin-related LM1 and LM3 got upregulated (normalised to 100% of WT signal; mean ± SD of three biological replicates; *P < 0.05; t-test). (**F**) Effect of galactan loss on auxin-induced bending capacity. The auxin-containing paste induced bending of the 1st internode in *siGALS3* plants. At least 7 independent plants were analysed.

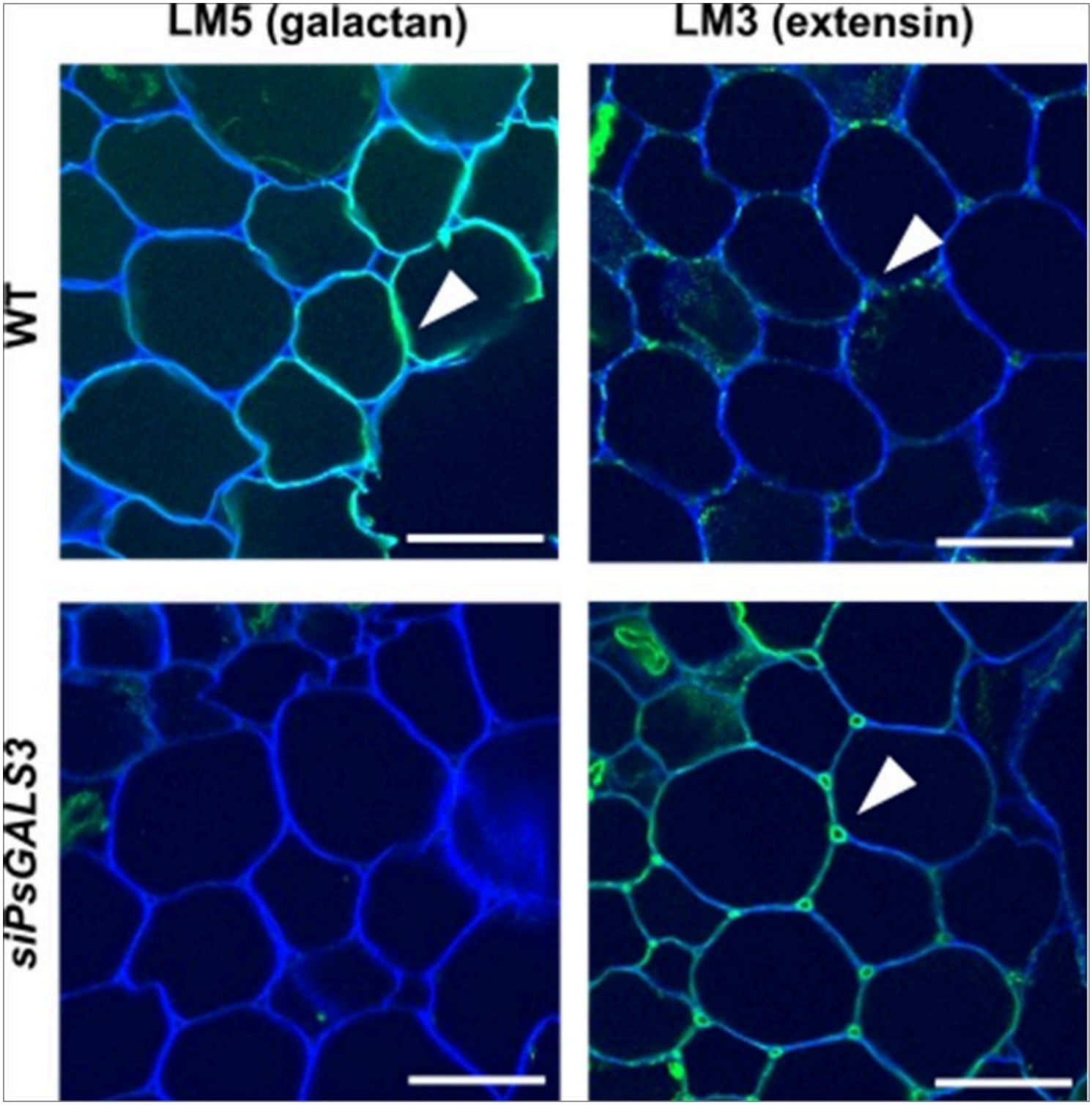

Figure 8

Immunolocalization of cell wall epitopes in pea stems of wild type (WT) and *siPsGALS3* plants. Transverse sections of the second internode were stained with LM5 (galactan), LM3 (extensin). Antibody-generated signals are shown in green, and Calcofluor White was used as a cell wall counterstain (blue). Arrowheads depict the signal. Note the loss of the LM5 signal and upregulation of the LM3 signal (triangular junctions) in the *siPsGALS3* plant. Scale bar = 20 μm.

Supplementary Files

This is a list of supplementary files associated with this preprint. Click to download.

- supplemtable1.docx